# Optical Cycling Functionalization of Arenes

Claire E. Dickerson,[†] Han Guo,[†] Guo-Zhu Zhu,[‡] Eric R. Hudson,[‡] Justin R. Caram,[†] Wesley C. Campbell,[‡] and Anastassia N. Alexandrova[*,†]

†*Department of Chemistry and Biochemistry, University of California Los Angeles*

‡*Department of Physics and Astronomy, University of California Los Angeles*

E-mail: ana@chem.ucla.edu

**Abstract**

Closed, laser-induced optical transitions ("optical cycling transitions") of molecules can be used for state preparation and measurement in quantum information science and quantum sensing. Increasingly complex molecular species supporting optical cycling can provide new capabilities for quantum science, and it is not clear if there is a limit on their size or complexity. We explore Ca-O-L molecular constructs for supporting the optical cycling center, Ca, with ligands, L, being arenes. We find that L can be as large as coronene (i.e. $CaOC_{24}H_{11}$), without losing the diagonality of the Franck-Condon factor (FCF). Further, L can be substituted with electron-withdrawing groups to improve the FCF. Larger L, beyond $\approx$ 7 rings, can disrupt the diagonality of the FCF by closing the electronic state gap and mixing with the local states on the cycling center. Overall, we find that optical cycling can be retained for arenes, and offer a principle of their design.

# Graphical TOC Entry

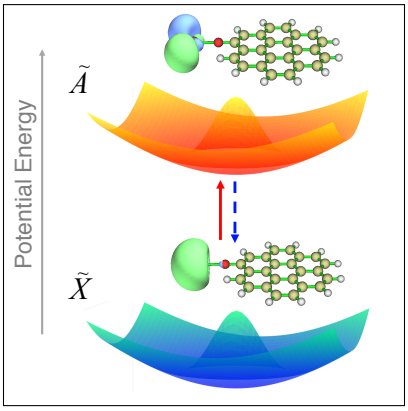


# Keywords

Optical Cycling, Atom-based qubits, Alkaline earth radicals, Substituted arenes, Theory

The field of experimental quantum information science is built on materials and molecules that would feature easily prepared and measured two-level systems, such as spin states, for utilization as qubits. Currently, superconducting qubits and trapped atomic species arguably lead this quantum hardware race. Atoms and atom-like molecular moieties with optically-induced, closed transitions have been explored in the field of atomic physics, particularly in the context of laser cooling, for quantum computation, analog quantum simulation and precision measurement.[1] Recently, an extension of such optical cycling centers toward larger polyatomic molecules has been realized in the laboratory. First, optical cycling was demonstrated with CaOH and $CaOCH_3$.[2–4] Even larger molecules, such as calcium phenoxides, have been proposed theoretically.[5,6] It is currently an open question whether the optical cycling of functionalized molecules can be engineered so that the Franck-Condon factor (FCF) can be retained in the large molecule limit, *i.e.* where the molecular ligand grows beyond a size where its details no longer affect the optical cycling. Should this prove possible, it would open the door to adding modularized quantum state readout to any substrate to which such a ligand can be attached.

In this contribution, we show that the ligand, L, in Ca-O-L can grow beyond a single carbon ring to larger arenes. This is possible because the geometries of arenes are relatively rigid and their electronic states feature substantial gaps in their highest occupied molecular orbitals (HOMO) to lowest unoccupied molecular orbitals (LUMO), which do not mix with the states on Ca, because they belong to a different irreducible representation in the $C_s$ point group (i.e. they are perpendicular to the molecular plane). The energies of the electronic states of arenes are also easily tuned by electron-withdrawing substitutions on the ring and via arene size.

Conveniently for this investigation, arenes are abundant throughout the universe,[7–10] and extensively characterized by, for example, infrared (IR) spectroscopy.[11] Databases exist containing vibrational harmonic spectra for arenes, namely polycyclic aromatic hydrocarbons, up to hundreds of carbon atoms.[12,13] Thus, the extension toward application of arenes in

optical cycling benefits from existing insights from laser cooling molecules and knowledge of extensive arene IR vibrational spectra. In other words, much of the groundwork necessary for adding optical cycling centers to arenes for quantum measurements and computing is already in place.

Previously, identifying optically cyclable molecules required either finding spectrocopic properties (such as diagonal FCFs) in the literature, or by trial and error. However, recently, some design strategies have emerged. Ivanov *et al.* showed that an alkaline earth metal radical can be attached to phenyl, cyclopentadienyl, and pyrrolide, and the metal could retain some optical cycling capabilities.[5] Additionally, they showed multiple optical cycling radicals could be attached to the same ligand if they are sufficiently spaced.[14] In a recent study, we showed that a cycling Ca or Sr radical attached to a phenoxide can have its diagonal FCF boosted by chemical substitution on the far side of the carbon ring.[6] The underlying design principle that this revealed, when the electronic transition is isolated on a metal radical, is that the FCF responds to the nature of the substituents in a manner predicted by the sum of the substituents' Hammett parameters. Specifically, electron-withdrawing groups spatially isolated from the cycling center increase the diagonality of the FCF by symmetrizing the ground and excited state potential energy surfaces, where the largest off-diagonal decay is the Ca-O stretching mode.

This earlier work led us to realize that the ligand HOMO-LUMO gap might play an important role in keeping the electronic states of the cycling center and the associated transition isolated. Here, we hypothesize that the HOMO-LUMO gap is one of the key design parameters for larger molecules that can support optical cycling centers with diagonal FCF. We explore this possibility on the basis of the Ca-O-L platform, where L is an arene. Arenes are rigid molecules, so their HOMO-LUMO gap can be reliably modified via the number of conjugated aromatic rings. Therefore, we explore arene ligands of increasing size, from naphthalene to ovalene, and then take it to the large-ligand-limit simulated by a graphene edge. In this way we expose the L's HOMO-LUMO gap as an important design consid-

eration for expanding the repertoire of L for optical cycling. We additionally explore the relative orientation of L and Ca (or Ca-O placement on the arene rings), as well as further fuctionalization of arenes with fluorines, which was previously shown to help diagonalize the FCF in Ca and Sr phenoxides.[6] All studied molecules are shown in Figure 1.

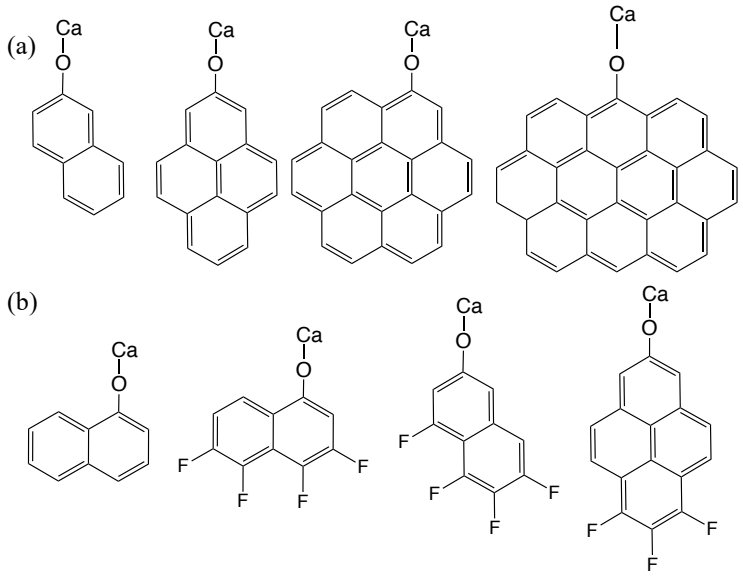


Figure 1: Arenes decorated with optical cycling motifs that are considered in this study. Row (a) from left to right: naphthalene, pyrene, coronene, ovalene. Row (b): h-naphthalene ("h" stands for "horizontal"), and fluorinated derivatives (F-h-naphthalene, F-naphtalene, F-pyrene).

For a species to host an optical cycling transition, the first electronic excitation must be exceptionally vertical and feature minimal vibrational leakage channels for non-radiative decay. The transition also needs to be isolated from other excitations and lie below the dissociation threshold. For the vertical transition, it is advantageous for both the ground and the excited state densities to be localized on the cycling center (in this work, the Ca radical) in Ca-O-L, and feature minimal (and equal) amount of Ca-O bond covalency. The natural transition orbitals (NTOs) of the HOMO ($\tilde{X}$) and LUMO ($\tilde{A}$) for naphthalene and coronene can be seen in Figure 2. The electron density remains isolated on the metal, with a very small contribution from the oxygen. The Ca-O bond ionicity is confirmed for the ground states via natural population analysis (NPA) (see Table 1). These results suggest

that all molecules feature highly-ionic Ca-O bonds, and the ionicity increased slightly upon fluorination.

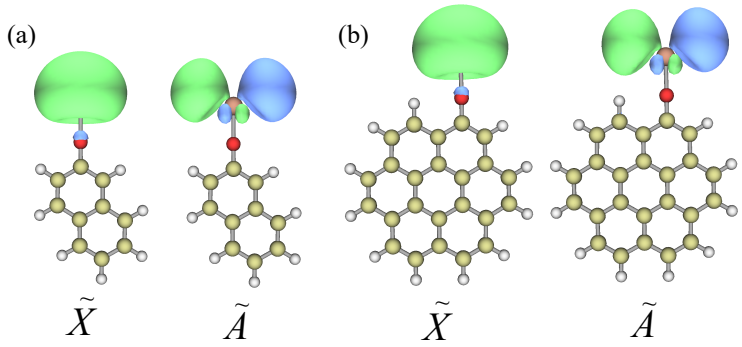


Figure 2: CaO-functionalized naphthalene and coronene NTOs of the ground to first excited state transition ($\tilde{X} \rightarrow \tilde{A}$) with an isosurface value of 0.03. No electron density can be found far from the calcium.

**Table 1: Computed NPA charges on Ca and O for all molecules' ground states.**

| Substituent | Charge (Ca) | Charge (O) |
|---|---|---|
| h-naphthalene | 0.96077 | -1.05630 |
| F-h-naphth | 0.96053 | -1.03787 |
| naphthalene | 0.95817 | -1.06100 |
| pyrene | 0.95924 | -1.06000 |
| coronene | 0.96138 | -1.04898 |
| ovalene | 0.96578 | -1.03405 |
| F-naphth | 0.96086 | -1.04382 |
| F-pyrene | 1.00522 | -1.09231 |

Next, we explore the similarity between the ground and first excited potential energy surfaces (Table 2). Ca-O bond length changes between the minimum on the ground state surface and the minimum on the excited state surface are below 0.02 Å for all considered species. The bond length change becomes smaller upon fluorination, consistent with the increasingly isolated character of the radical and in accordance with the design principle introduced in ref.[6] Also, we find that the placement of the O-Ca moiety on the arene plays a role in that the "horizontal" derivatives feature poorer symmetries between the ground and the excited state surfaces.

Although the unpaired electron is localized on the metal throughout the transition, there

**Table 2: FCFs and Ca-O bond length change (excited state - ground state) for all molecules.**

| Substituent | FCF | Ca-O Change (Å) |
|---|---|---|
| h-naphthalene | 0.931 | -0.0163 |
| F-h-naphth | 0.917 | -0.0133 |
| naphthalene | 0.958 | -0.0163 |
| pyrene | 0.947 | 0.0164 |
| coronene | 0.931 | -0.0140 |
| ovalene | 0.167 | -0.0010 |
| F-naphth | 0.968 | -0.0127 |
| F-pyrene | 0.962 | -0.0151 |

is a nearly linear decrease in FCF as the arene ligand increases in size from naphthalene to coronene. The decrease can be related to the slight decrease in the isolated character of the frontier orbitals on the cycling molecules (Figure 3). As the arene gets larger, its intrinsic HOMO-LUMO gap (which, for example, in pyrene corresponds to the HOMO-1-LUMO+1 gap, shown in blue in Figure 3), closes, and approaches the metal-based electronic transition (shown in black in Figure 3). The ligand and Ca lowest unoccupied orbitals become particularly close as the arene increases in size. While FCFs can be improved slightly by substituting electron-withdrawing groups on the ligand, once L becomes ovalene, the verticality of the transition is lost due to excited state order switch, whereby the LUMO becomes an arene-centered orbital, as seen in Figure 3. Fluorinating these species systematically shifted all energy levels lower in energy, but the relative HOMO-LUMO gaps remained similar to their unsubstituted versions (see Supporting Information).

The HOMO-LUMO gap of the "ligands", where the electron density is not on the metal but solely on the arene molecule, are shifted, but still close to experimental electronic excitation energies of their singlet, neutral counterparts. These neutral species' electronic excitations were also benchmarked against the experiment,[15–17] using our computational methodology (see Supporting Information).

From a vibrational mode perspective, the dominant off-diagonal decay mode changes depending on the arene size and ligand symmetry (Figure 4). In naphthalene, the first two

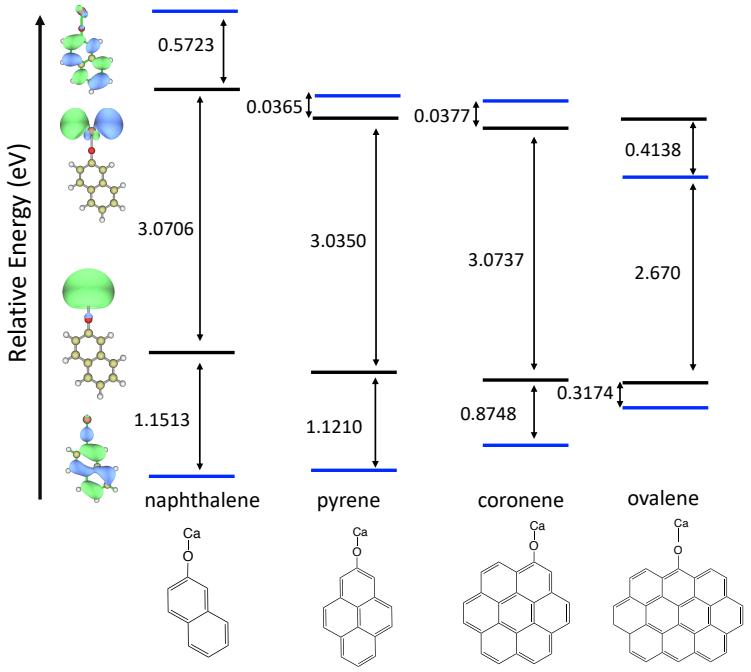


Figure 3: DFT energies of electron density localized on the ligand, or "ligand HOMO-LUMO" gap (blue), and density localized on the metal, or "metal HOMO-LUMO gap" (black), for naphthalene, pyrene, coronene, and ovalene. As ligand size increases, the ligand HOMO-LUMO gap decreases and approaches the isolated metal-metal electronic transition, until the transition is disrupted by the switching of the metal and ligand LUMOs, as seen in ovalene.

off-diagonal modes are the symmetric Ca-O stretch, and a Ca-O bend and stretch. However, with coronene, the dominant off-diagonal mode is the Ca-O in-plane bending, followed by Ca-O symmetric stretch. This could be due to the interaction of the unpaired electron on Ca with the delocalized electronic states on the arene; these states have a greater spatial overlap in the "horizontal" variants, and better match in energy with larger arenes. As such, increasing arene size disrupts the symmetric stretch mode and causes reduced symmetry between the ground and excited state potential energy surfaces. We can also conclude that placing the cycling centre on a $C_6$-ring that is more isolated from the rest of the polyaromatic system of the arene helps diagonalize the FCF for the same reason.

The FCF decrease can be mitigated slightly by adding electron-withdrawing groups in positions on the arenes such that the Ca-O symmetric stretch behavior is favored (i.e. far away from Ca-O) (see Table 2 and Figure 5). The substituted F-versions of the molecules

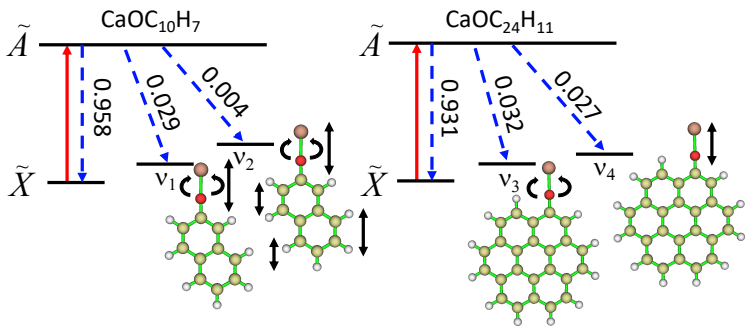


Figure 4: Photon cycling scheme with an excitation (red) to the first excited electronic state and decay (blue) to the ground electronic state for naphthalene and coronene. The FCFs are shown along with each decay pathway.

designed in this way have more symmetric ground and excited state potential energy surfaces, and thus, larger FCFs than unsusbtituted arenes. Electron-withdrawing to improve the symmetry of potential energy surfaces is described in more detail in the reference.[6]

Intriguingly, we find that for the "horizontal" arene ligands, where the in-plane bend mode is already the dominant vibrational leakage channel, fluorination does not help diagonalize the FCF (Table 2 and 5). When fluorines are substituted, FCFs decrease, and the bend off-diagonal decay increases to 0.05. Therefore, yet again the "vertical" arene ligands are more favorable than "horizontal" arene ligands for optical cycling.

Since increasing arene ligand size appears to lead to the eventual destruction of diagonal FCFs, we pushed the concept to its limit and examined Ca-O bound to the edge of 2D graphene. We consider two edge structures (Figure 6): in E1, Ca-O-C maintains a locally linear structure on the ground electronic state, while in E2, Ca-O-C is bent with an angle of 163.9°, due to the asymmetric local structure and charge density.

In the density of states (DOS) calculations, we see density mixing on graphene and the metal, for both structures, and both for the ground and excited states. This will disrupt the clean transitions, leading to poor FCFs. This is further illustrated by the plots of the charge density, showing the lack of localization and the spread of the charge density throughout the graphene edge. The orbitals of Ca mix with C orbitals, and split into two mixed orbitals. Thus, while functionalization of large-band-gap diamond with M-O optical cycling centers

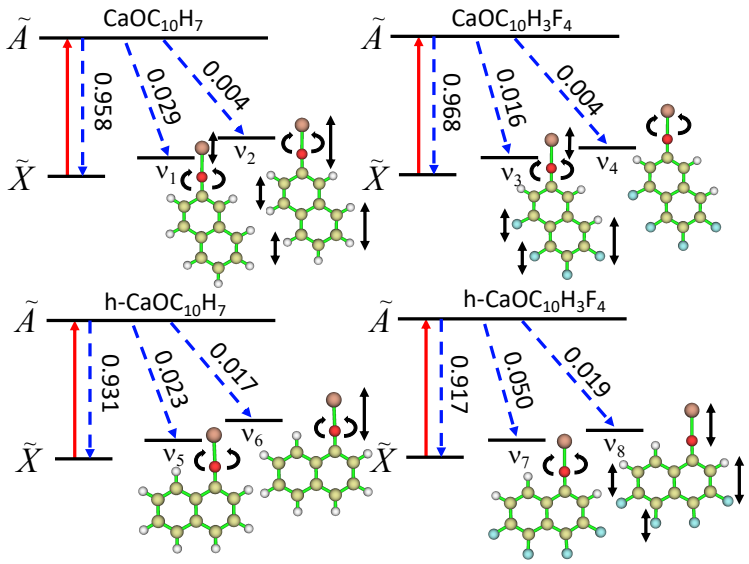


Figure 5: Photon cycling scheme with an excitation (red) to the first excited electronic state and decay (blue) to the ground electronic state for, from left to right: "vertical" naphthalene, "vertical" fluorinated naphthalene, "horizontal" naphthalene and "horizontal" fluorinated naphthalene. The FCFs are shown along with each decay.

was proposed to be possible,[18] the graphene edge is not a suitable substrate for this purpose. This is explained by the ligand band gap paradigm proposed in this work.

Finally, how could one synthesize such large molecules as arenes functionalized with optical cycling centers? Experimentally, various methods have been developed to produce the alkaline-earth-radical containing molecules, via reactions of the metal atoms with the volatile ligands.[3,4,19] The metal atoms are generated either by evaporation in a Broida-type oven[19] or by laser ablation of the metal targets. The atoms then react with the gaseous precursors to form the products. The reaction rate can be enhanced when pumping the ground-state metal atoms to the metastable excited states. Supersonic jet and cryogenic buffer-gas cooling[3,4] are commonly employed to make products vibrationally and rotationally cold. The functionalized arenes discussed here can be produced using similar method. Take CaO-naphthalene as an example, a nanosecond 1064 nm Nd:YAG laser is used to ablate the calcium target producing Ca atoms. Since the ligand, 2-naphthol, is involatile and has a melting point around 120 °C, a heated source is used to melt the 2-naphthol to generate enough vapor, which is entrained in a cryogenic buffer gas of Ne to react with Ca atoms.

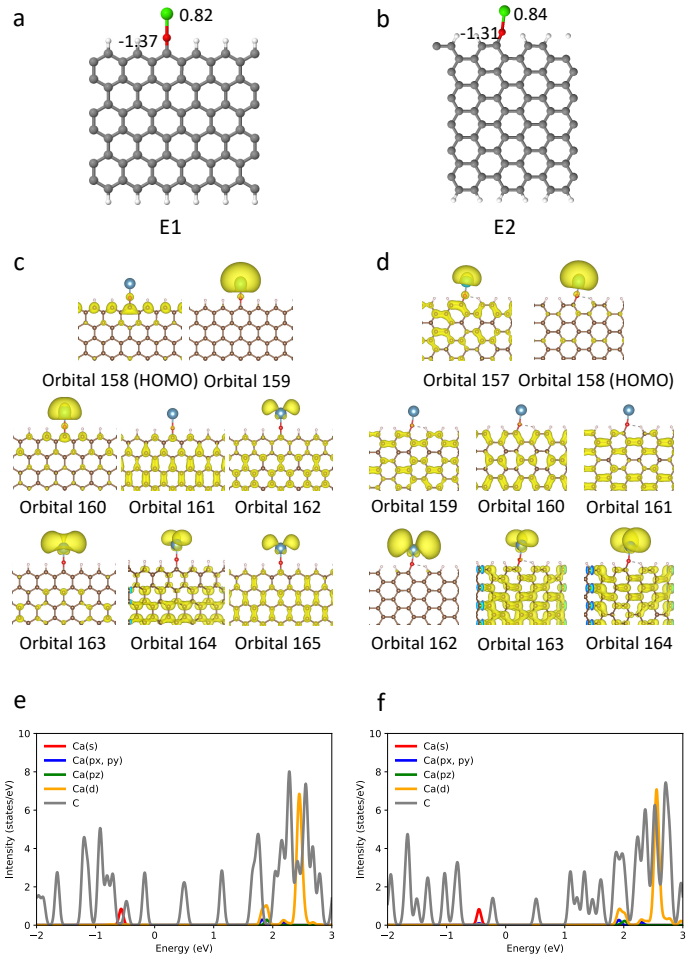


Figure 6: (a) (b) Optimized ground state structures for two edge structures, E1 and E2. The atomic charges on Ca and O from the Bader charge analysis are also shown. (c) (d) Electron density of molecular orbitals for CaO supported on two graphene edges. The isosurfaces are plotted with an isovalue of 0.001. (e) (f) PDOS for CaO supported on two graphene edges.

The formed CaO-naphthalene can be probed by the laser spectroscopy.

To conclude, in this work it was found that arene ligands attached to a linear Ca-O could be suitable for optical cycling. We propose a design strategy and a way to foresee the limit on the molecular size permitting to preserve optical cycling. The cycling functionality of these large molecules is dependent on the size of the arene and its orientation with respect to the Ca-O center. As the arene ligand grows, its intrinsic HOMO-LUMO gap becomes smaller and encourages electronic state mixing with the states of the cycling center, and vibrational mode mixing. These effects produce asymmetric ground and excited state potential energy surfaces

and less diagonal FCF. Extending arenes all the way to ovalene or graphene destroyed the clean electronic transition in this way, as the graphene edge states mixed with the electronic transition in CaO-graphene, and the ligand LUMO switched with the metal LUMO in CaO-ovalene. An arene as large as coronene is predicted to be a successful host for the Ca-O optical cycling center, being the largest such ligand proposed to date.

# Computational Methods

All molecular calculations in this work were done at the PBE0-D3/def2-TZVPPD level of theory[20–22] with DFT and time-dependent density functional theory (TD-DFT) on a superfine grid, using Gaussian16.[23] This level of theory was previously extensively benchmarked against multireference CAS-PT2 calculations for CaOH, SrOH, CaF, SrF, and $CaOCH_3$.[6] Additionally, electronic excitation energies for neutral naphthalene, pyrene, and coronene, computed with TD-DFT matched the experimental data within 0.04 eV (see Supporting Information). FCFs, including Duschinsky rotations, were calculated from harmonic vibrational frequencies. The harmonic approximation is expected to be reliable, because the optical center is well-isolated from the modes of the ligand, and the anharmonicity, if any, will be similar from the ground to excited state and should not affect the diagonality of the FCF, as we detailed previously for phenoxydes.[6] Also, for naphthalene, anthracene, and tetracene, the main anharmonic modes were the C-C or C-H stretches, in the 1300-1600 $cm^{-1}$ range,[24,25] i.e. sufficiently far from Ca-O stretching or bending modes (dominant contributors to the FCF), which are less than 700 $cm^{-1}$. Multiwfn[26] was used for molecular visualizations.

OCCs bound to the edge of a single-layer graphene were computed using VASP.[27–30] Geometry optimizations were carried out using PBE.[31,32] The hybrid functional, HSE06, was used for charge density and density of states calculations,,[33–35] as it has been previously benchmarked against experiment for the prediction of band gaps.[36,37] The interactions be-

tween the ionic cores and the electrons were described using the projector augmented-wave (PAW) potentials.[38,39] A $1 \times 4 \times 1$ Monkhorst-Pack k-point grid and a plane wave cutoff energy of 400 eV were employed. The 2D graphene sheet was represented as an infinite strap with periodic boundary conditions, in which the two edges were covered with H atoms, one of which was removed to deposit CaO. We used a large unit cell of 15Å $\times$ 15Å $\times$ 25Å to prevent the interaction between periodic images. The top three layers of C atoms and the top-edge H atoms were relaxed during the geometry optimization, with a convergence criterion of 0.01 eV/atom.

## Acknowledgement

This work was supported by the U.S. Department of Energy, Office of Science, Basic Energy Sciences, under Award #DE-SC0019245. Computational resources were provided by XSEDE.

## Supporting Information Available

Energy level diagrams for the fluorinated arenes, horizontal naphthalene, and TD-DFT benchmarking for the neutral, singlet species are included in the Supporting Information.

The Supporting Information is available free of charge at [Link Here].

## References

(1) DiVincenzo, D. P. The physical implementation of quantum computation. *Fortschritte der Physik: Progress of Physics* **2000**, *48*, 771–783.

(2) Brazier, C.; Ellingboe, L.; Kinsey-Nielsen, S.; Bernath, P. Laser spectroscopy of alkaline earth monoalkoxide free radicals. *J. Am. Chem. Soc.* **1986**, *108*, 2126–2132.

(3) Kozyryev, I.; Baum, L.; Matsuda, K.; Doyle, J. M. Proposal for Laser Cooling of Complex Polyatomic Molecules. *ChemPhysChem.* **2016**, *17*, 3641–3648.

(4) Kozyryev, I.; Steimle, T. C.; Yu, P.; Nguyen, D.-T.; Doyle, J. M. Determination of CaOH and CaOCH3 vibrational branching ratios for direct laser cooling and trapping. *New J. Phys.* **2019**, *21*, 052002.

(5) Ivanov, M. V.; Bangerter, F. H.; Wójcik, P.; Krylov, A. I. Toward Ultracold Organic Chemistry: Prospects of Laser Cooling Large Organic Molecules. *J. Phys. Chem. Lett.* **2020**, *11*, 6670–6676, PMID: 32787222.

(6) Dickerson, C. E.; Guo, H.; Shin, A. J.; Augenbraun, B. L.; Caram, J. R.; Campbell, W. C.; Alexandrova, A. N. Franck-Condon tuning of optical cycling centers by organic functionalization. *Phys. Rev. Lett.* **2021**, in press. arXiv:2010.04207.

(7) Snow, T. P.; Witt, A. N. The Interstellar Carbon Budget and the Role of Carbon in Dust and Large Molecules. *Science* **1995**, *270*, 1455–1460.

(8) Tielens, A. Interstellar Polycyclic Aromatic Hydrocarbon Molecules. *Annu. Rev. Astron. Astrophys.* **2008**, *46*, 289–337.

(9) Hardegree-Ullman, E.; Gudipati, M.; Boogert, A.; Lignell, H.; Allamandola, L. J.; Stapelfeldt, K. R.; Werner, M. *Astrophys. J.* **2014**, *784*, 172.

(10) Hanine, M.; Meng, Z.; Lu, S.; Xie, P.; Picaud, S.; Devel, M.; Wang, Z. Formation of Interstellar Complex Polycyclic Aromatic Hydrocarbons: Insights from Molecular Dynamics Simulations of Dehydrogenated Benzene. *Astrophys. J.* **2020**, *900*, 188.

(11) Young, E. T.; Becklin, E. E.; Marcum, P. M.; Roellig, T. L.; Buizer, J. M. D.; Herter, T. L.; Güsten, R.; Dunham, E. W.; Temi, P.; Andersson, B.-G. et al. Early Science with SOFIA, the Stratospheric Observatory for Infrared Astronomy. *Astrophys. J. Lett.* **2012**, *749*, L17.

(12) Bauschlicher, C. W.; Boersma, C.; Ricca, A.; Mattioda, A. L.; Cami, J.; Peeters, E.; de Armas, F. S.; Saborido, G. P.; Hudgins, D. M.; Allamandola, L. J. The NASA Ames Polycyclic Aromatic Hydrocarbon Infrared Spectroscopic Database: The Computed Spectra. *Astrophys. J. Suppl.* **2010**, *189*, 341–351.

(13) Malloci, G.; Joblin, C.; Mulas, G. Online database of the spectral properties of polycyclic aromatic hydrocarbons. *Chem. Phys.* **2007**, *332*, 353 – 359.

(14) Ivanov, M. V.; Gulania, S.; Krylov, A. I. Two Cycling Centers in One Molecule: Communication by Through-Bond Interactions and Entanglement of the Unpaired Electrons. *J. Phys. Chem. Lett.* **2020**, *11*, 1297–1304, PMID: 31973526.

(15) Berlman, I. *Handbook of fluorescence spectra of aromatic molecules*; Academic Press, 1971.

(16) Smyth, K. C.; Schiavone, J. A.; Freund, R. S. Excitation of fluorescence in naphthalene and azulene by electron impact. *J. Chem. Phys.* **1975**, *62*, 136–144.

(17) Novak, J.; Windsor, M. Laser photolysis and spectroscopy in the nanosecond time range: Excited singlet state absorption in coronene. *J. Chem. Phys.* **1967**, *47*, 3075–3076.

(18) Guo, H.; Dickerson, C. E.; Shin, A. J.; Zhao, C.; Atallah, T. L.; Caram, J. R.; Campbell, W. C.; Alexandrova, A. N. Surface chemical trapping of optical cycling centers. *Phys. Chem. Chem. Phys.* **2021**, *23*, 211–218.

(19) Ellis, A. M. Main group metal-ligand interactions in small molecules: new insights from laser spectroscopy. *Int. Rev. Phys. Chem.* **2001**, *20*, 551–590.

(20) Perdew, J. P.; Ernzerhof, M.; Burke, K. Rationale for mixing exact exchange with density functional approximations. *J. Chem. Phys.* **1996**, *105*, 9982–9985.

(21) Grimme, S.; Anthony, J.; Ehrlich, S.; Krieg, H. A consistent and accurate ab initio

parametrization of density functional dispersion correction (DFT-D) for the 94 elements H-Pu. *J. Chem. Phys.* **2010**, *132*, 154104.

(22) Rappoport, D.; Furche, F. Property-optimized gaussian basis sets for molecular response calculations. *J. Chem. Phys.* **2010**, *133*, 134105–1–134105–11.

(23) Frisch, M. J.; Trucks, G. W.; Schlegel, H. B.; Scuseria, G. E.; Robb, M. A.; Cheeseman, J. R.; Scalmani, G.; Barone, V.; Petersson, G. A.; Nakatsuji, H. et al. Gaussian16 Revision C.01. 2016; Gaussian Inc. Wallingford CT.

(24) Cané, E.; Miani, A.; Trombetti, A. Anharmonic Force Fields of Naphthalene-h 8 and Naphthalene-d 8. *J. Phys. Chem. A* **2007**, *111*, 8218–8222, PMID: 17672437.

(25) Mackie, C. J.; Candian, A.; Huang, X.; Maltseva, E.; Petrignani, A.; Oomens, J.; Buma, W. J.; Lee, T. J.; Tielens, A. G. G. M. The anharmonic quartic force field infrared spectra of three polycyclic aromatic hydrocarbons: Naphthalene, anthracene, and tetracene. *J. Chem. Phys.* **2015**, *143*, 224314.

(26) Lu, F., T.; Chen Multiwfn: A multifunctional wavefunction analyzer. *J. Comput. Chem.* **2012**, *33*, 580–592.

(27) Kresse, G.; Furthmüller, J. Efficient iterative schemes for ab initio total-energy calculations using a plane-wave basis set. *Phys. Rev. B* **1996**, *54*, 11169–11186.

(28) Kresse, G.; Furthmüller, J. Efficiency of ab-initio total energy calculations for metals and semiconductors using a plane-wave basis set. *Comput. Mater. Sci.* **1996**, *6*, 15 – 50.

(29) Kresse, G.; Hafner, J. Ab initio molecular-dynamics simulation of the liquid-metal–amorphous-semiconductor transition in germanium. *Phys. Rev. B* **1994**, *49*, 14251–14269.

(30) Kresse, G.; Hafner, J. Ab initio molecular dynamics for liquid metals. *Phys. Rev. B* **1993**, *47*, 558–561.

(31) Perdew, J. P.; Burke, K.; Ernzerhof, M. Generalized Gradient Approximation Made Simple. *Phys. Rev. Lett.* **1997**, *78*, 1396–1396.

(32) Perdew, J. P.; Burke, K.; Ernzerhof, M. Generalized Gradient Approximation Made Simple. *Phys. Rev. Lett.* **1996**, *77*, 3865–3868.

(33) Krukau, A. V.; Vydrov, O. A.; Izmaylov, A. F.; Scuseria, G. E. Influence of the exchange screening parameter on the performance of screened hybrid functionals. *J. Chem. Phys.* **2006**, *125*, 224106.

(34) Tang, W.; Sanville, E.; Henkelman, G. A grid-based Bader analysis algorithm without lattice bias. *J. Phys. Condens. Matter* **2009**, *21*, 084204.

(35) Henkelman, G.; Arnaldsson, A.; Jónsson, H. A fast and robust algorithm for Bader decomposition of charge density. *Comput. Mater. Sci.* **2006**, *36*, 354 – 360.

(36) Borlido, P.; Aull, T.; Huran, A.; Tran, F.; Marques, M. A. L.; Botti, S. *J. Chem. Theory Comput.* **2019**, *15*, 5069–5079.

(37) Borlido, P.; Schmidt, J.; Huran, A. W.; Tran, F.; Marques, M. A. L.; Botti, S. *npj Comput. Mater.* **2020**, *6*, 96.

(38) Kresse, G.; Joubert, D. From ultrasoft pseudopotentials to the projector augmented-wave method. *Phys. Rev. B* **1999**, *59*, 1758–1775.

(39) Blöchl, P. E. Projector augmented-wave method. *Phys. Rev. B* **1994**, *50*, 17953–17979.